Supporting Information

Ultraviolet refractive index values of organic aerosol extracted from deciduous forestry, urban and marine environments

Connor R. Barker,[a,b] Megan Poole,[a] Matthew Wilkinson,[c] James Morison,[c] Alan Wilson,[d] Gina Little,[d] Edward J. Stuckey,[a,e] Andrew D. Ward,[b,*] and Martin D. King[a,*]

AUTHOR ADDRESS

[a] Department of Earth Sciences, Centre of Climate, Ocean and Atmospheres, Queens Building, Royal Holloway University of London, Egham, Surrey, TW20 0EX, U.K.

[b] STFC, Central Laser Facility, Research Complex at Harwell, Rutherford Appleton Laboratory, Didcot, Oxfordshire, OX11 0FA, U.K.

[c] Centre for Sustainable Forestry and Climate Change, Forest Research, Alice Holt Lodge, Farnham, Surrey, GU10 4LH, U.K.

[d] Environment and Climate Change Canada, 45 Alderney Dr, Dartmouth, Nova Scotia, B2Y 2N6, Canada

[e] ISIS Pulsed Neutron and Muon Source, Rutherford Appleton Laboratory, Oxford, OX11 0QX, UK

CORRESPONDING AUTHOR

*E-mail: m.king@rhul.ac.uk

Phone: +441784 414038

Contents

SAMPLE DETAILS

Table 1: The constituent months for each sample studied

Sample	Months
Polluted Urban Spring	Apr 18
Polluted Urban Summer	Aug 17
Polluted Urban Autumn	Sep-Nov 19
Polluted Urban Winter	Jan-Feb 18
Remote Marine Autumn	Sep-Nov 18
Remote Marine Winter	Dec 2018-Feb 2019
Forestry Below Canopy Autumn	Aug-Sep, Nov 2018
Forestry Above Canopy Spring	Apr-May 2019
Forestry Above Canopy Summer	Jul-Aug 2019
Forestry Above Canopy Autumn	Aug-Sep, Nov 2018

CONTROL SAMPLES

Predominantly organic aerosol samples as in this study are likely to form a thin film at an air-water interface [1]. Measurement of surface pressure-area compression isotherms can indicate the presence (or lack thereof) of organic material in the chloroform solvent. A polytetrafluoroethylene (PTFE) Langmuir trough (NIMA) was used to record surface pressure-area isotherms of the August, September and November 2018 Forestry samples, each comprising of a blank filter sample, an in-canopy sample, and an above canopy sample. In the optical trapping experiments, the three monthly samples were combined into one seasonal sample from each environment. 100 µL of each sample was spread onto the surface of an deionised aqueous subphase (18.2 MΩ cm^{-1}) using a µL Hamilton syringe to form a thin film at the interface, which was then left for several minutes to allow the chloroform solvent from the sample to fully evaporate. Compression isotherms were performed at a speed of 25 cm^2 min^{-1} at a temperature of ~20 °C, from areas of 231-48 cm^2, using the supplied NIMA propriety software. The surface pressure was recorded using a Wilhelmy plate. The isotherms for the real organic tropospheric extracts from above and in the canopy all show an increase in surface pressure at low area (Fig. S1), indicating the presence of organic material. Adversely, the blue curves displaying the isotherms of the blank samples show very little or no increase in surface pressure at low area, demonstrating that no organic material is present on the blank filters and confirming the validity of the real tropospheric aerosol samples. In addition, the variable slope and surface pressure at the minimum area demonstrate the variation in chemical composition between the samples.

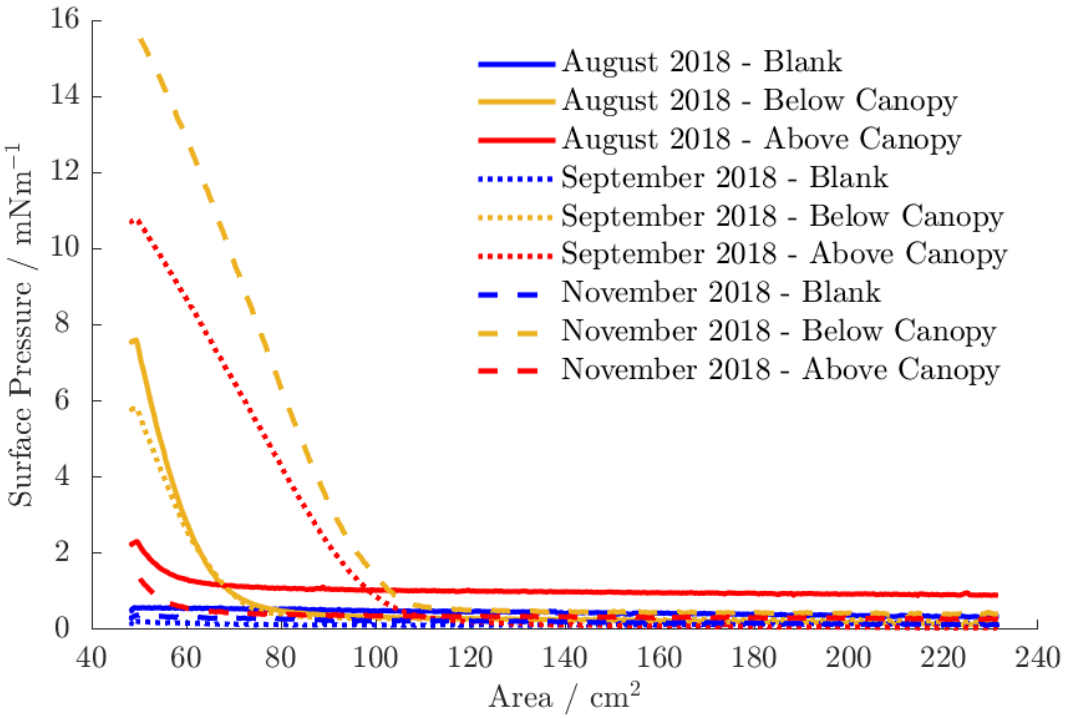

Figure S1: Isotherms of surface pressure against area for the Autumn Forestry samples, recorded using a Langmuir trough. The yellow and red curves demonstrate the isotherms for the samples taken in and above the canopy respectively. The blue curves are for the blank samples containing no aerosol material.

MIE FITTING PROCESSES

An array of calculated spectra were produced over iterations of *A*, *B*, *C*, and *r* in bounded ranges. The optically trapped particles were assumed to be homogeneous spheres in air (n_{medium}=1.00027 at λ=0.450 μm under experimental conditions [2]). The scattering was calculated over a 30° cone angle, equivalent to a solid angle of 0.84 sr, through integration of the scattering angle, θ, over 150-180° ($\Delta\theta$=0.5°). The optimal values of *A*, *B*, *C*, and *r* were determined by minimising the averaged absolute differences in the wavelength positions of the MDRs between the experimental spectrum and each calculated spectra. A second fitting stage analysed the refractive indices of each individual MDR wavelength position for 21 radii of $r_{bestfit}$±0.02 μm through iteration of the *A* parameter, with *B* and *C* fixed at the previous best fit values. For a given radius, each MDR was analysed sequentially, with the value of *A* varied as ±0.005 around an estimated value to minimise the value of $\Delta\theta$ between the experimental and calculated MDR. The resulting data set of wavelength-resolved refractive indices was fitted to a Cauchy equation using a Trust Region Reflective algorithm [3]. The optimal particle radius, and therefore the optimal refractive index dispersion. was determined by minimising the value of the fitting coefficient, δ, which combines the one standard deviation errors in the *A*, *B*, and *C* parameters across *j* MDRs in the spectrum:

$$\delta = \frac{1}{j}\sqrt{\sum_{i=1}^{j} \Delta A^2 + \frac{\Delta B^2}{\lambda_i^2} + \frac{\Delta C^2}{\lambda_i^4}} \qquad \text{(S1)}$$

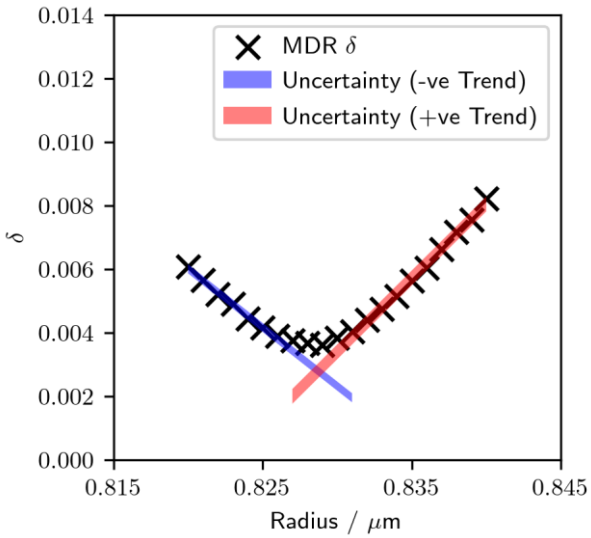

Figure S2: A representative plot of the fitting coefficient, δ (Eq. S1), vs. the estimated radius of the particle, *r* for polluted urban (autumn) aerosol. The blue and red shaded regions represent the two standard deviations uncertainty in the negative and positive linear trends respectively. The uncertainty in the radius (here *r*=±*0*.0009) is calculated as the width of the diamond where the shaded regions overlap.

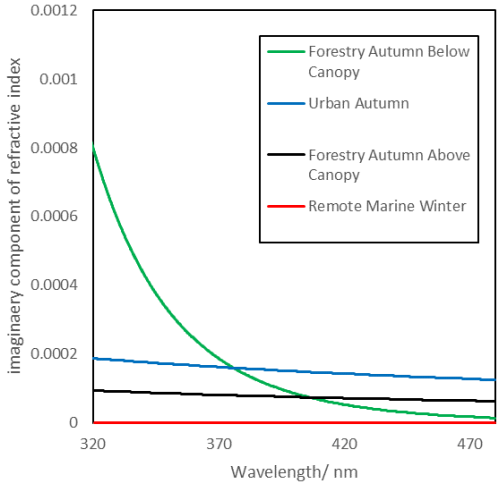

Figure S3: The imaginary component of refractive index as a function of wavelength used to match the calculated intensities to the measured intensities for the spectra shown in Fig 2. Urban Autumn

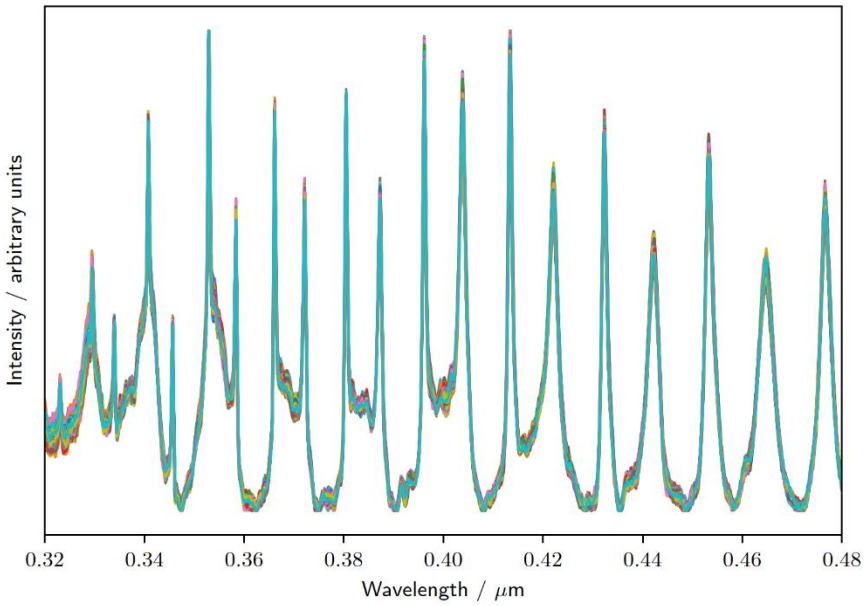

Figure S4: A time series of spectra taken from a 240 frame capture at 1 frame per second for a the Urban Autumn sample. No significant changes were observed in this timeframe.

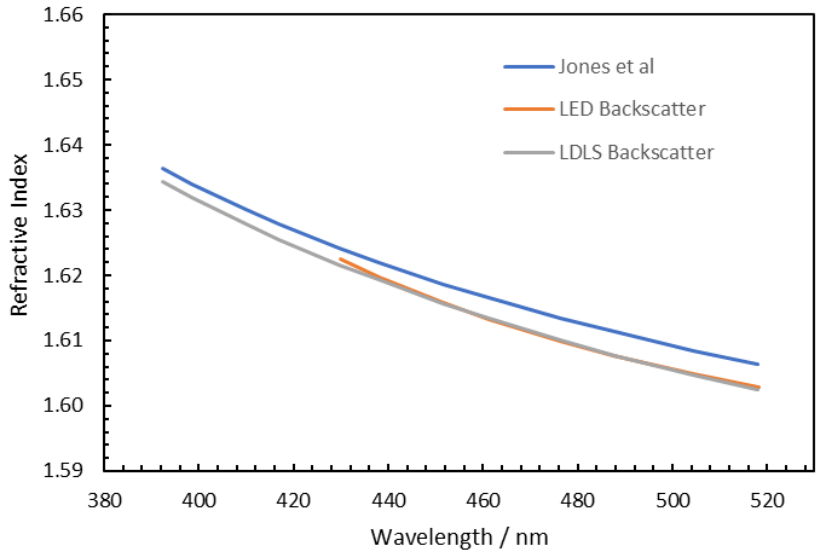

Figure S5: To assess for systematic bias between the work reported by Shepherd et al (4) and this work the optics on the optical trapping microscope were re-configured to permit dual collection of a backscattered LED using the lower trapping objective (see Figure 1) and backscattered LDLS using a side objective as described in the Methods section. A single polystyrene particle (Invitrogen) was captured and the Mie spectrum from both techniques was analysed for the same particle. The minimum in uncertainty (see S2) was at a radius 0.895 microns radius for both spectra. The plot above shows the dispersion of refractive index with wavelength for (blue) average from Jones et al. (7) extrapolated to wavelengths below 480 nm, (orange) LED illuminated polystyrene bead (as per Shepherd et al. (6)) and (grey) LDLS UV illuminated polystyrene bead (this work).

ATMOSPHERIC IMPLICATIONS

Table 2: the calculated wavelength dependent complex refractive index components for urban and remote aerosol, estimated using measurements from this work and others[4,5,6]

Environment	Wavelength (nm)	n	iκ
Urban	320	1.5232	0.2845
	400	1.5046	0.1457
	500	1.4926	0.0746
	600	1.4861	0.0432
	700	1.4822	0.0272
	785	1.4800	0.0192
Remote	320	1.4522	0.0067
	400	1.4516	0.0061
	500	1.4511	0.0056
	600	1.4510	0.0052
	700	1.4508	0.0049
	785	1.4507	0.0047

A complex refractive index was calculated for the organic portion of a core shell aerosol, the results of which are presented in table x. The real component of the refractive index, n, was produced by fitting a Cauchy equation using both the data presented here and in Shepherd et al[4]. The datasets were displaced equidistantly with n before the following two-term Cauchy equations were fit:

$$n_{\mathrm{Urban}} = 1.4714 + \frac{5.3091 \times 10^3}{\lambda^2}$$

$$n_{\mathrm{Remote}} = 1.4504 + \frac{1.9230 \times 10^2}{\lambda^2}$$

The imaginary refractive index, iκ , was produced by applying existing optical measurements of organic aerosol to the forumla:

$$i\kappa = \frac{\sigma\lambda(\frac{\lambda}{\lambda_0})^{-\alpha}}{4\pi}$$

Where σ is the absorption coefficient, α the angstrom exponent and λ0 is the wavelength that secondary measurements were taken at by Kirkstetter et al[5], and Virkkula et al[6].

REFERENCES

(1) P. S. Gill, T. E. Graedel, C. J. Weschler, Rev. Geophys. **1983**, 21 (4), 903–920. https://doi.org/10.1029/RG021i004p00903.
(2) P. E. Ciddor, Appl. Opt. **1996**, 35 (9), 1566–1573. https://doi.org/10.1364/AO.35.001566.
(3) M. A. Branch, T. F. Coleman, Y. A. Li, SIAM J. Sci. Comput. **1999**, 21 (1), 1–23. https://doi.org/10.1137/S1064827595289108.
(4) R. H. Shepherd, M. D. King, A. A. Marks, N. Brough and A. D. Ward, Atmospheric Chemistry and Physics, **2018**, 18, 5235–5252.
(5) T. W. Kirchstetter, T. Novakov and P. V. Hobbs, Journal of Geophysical Research: Atmospheres, **2004**, 109, 1–12.
(6) A. Virkkula, H. Grythe, J. Backman, T. Petäjä, M. Busetto, C. Lanconelli, A. Lupi, S. Becagli, R. Traversi, M. Severi, V. Vitale, P. Sheridan and E. Andrews, Atmospheric Chemistry and Physics, **2022**, 22, 5033–5069
(7) S. H. Jones, M. D. King and A. D. Ward, Physical Chemistry Chemical Physics, **2013**, 15, 20735–20741